Sensors and Materials, Vol. 19, No. 2 (2007) 079–094
MYU Tokyo

S & M 0667

Bending Characterization of Electroplated Nickel Microbeams

Chingfu Tsou*, Hungchung Li, Tenghsien Lai,
Changchun Hsu[1] and Weileun Feng[1]

Department of Automatic Control Engineering, Feng Chia University, Taichung, Taiwan
[1]Power Mechanical Engineering Department, National Tsing Hua University,
Hsinchu, Taiwan

(Received January 4, 2006; accepted March 15, 2007)

Key words: bending, microcantilever, creep, electroplated nickel, MEMS

In this study, we aim to investigate the mechanical behavior of an electroplated nickel film using the bending micromachined cantilever approach. The bending test, including quasi-static, reloading, and time-dependent creep was performed using a nanoindentation loading system. The mechanical properties of Young's modulus and yielding strength were determined through bending testing, and the experimental average values are 191 GPa and 0.79 GPa, respectively. In addition, by measuring the load-deflection of a microcantilever under various stress levels with a constant temperature, the bending creep behavior of the electroplated nickel film was determined and characterized. Experimental results show that when bending stress is smaller than the measured yielding strength, the relation between stress and strain rates can be expressed as $(d\varepsilon/dt) = 0.0016e^{2.5(\sigma)}$. These test results can provide the basis for the design optimization of nickel microstructure. Thus, the performance and reliability of MEMS/IC devices can be predicted and improved.

1. Introduction

A German acronym for Lithographie, Galvanoformung. and Abformung (LIGA)-like processes have been developed in recent years as a means of producing metal microstructures in several micrometers up to a hundred micrometers thick ranges for microelectromechanical systems (MEMS). In particular, the nickel microstructure fabricated by electroplating has the advantages of low-residual stress, high density, and superior mechanical strength and can be formed as a high-aspect-ratio microstructure by photolithography. Consequently, electroplated nickel films and their mechanical

*Corresponding author, e-mail address: cftsou@fcu.edu.tw

behavior are of significant interest to MEMS community.[1–4] However, the electroplating of nickel presents several processing issues that affect its mechanical properties. For example, a fabricated nickel film by electroplating is very sensitive to deposition conditions which cause significant processing lot variations of mechanical properties.[5–9] Previous researches also reported that the mechanical properties of thin film materials usually vary with the fabrication process, such as film thickness, and are not the same as those of bulk one's.[10–15] Furthermore, thin film mechanical properties not only affect mechanical performance but also the electrical as well as the optical performance of microdevices. Importantly, the reliability of time dependence is a critical issue for practical application and the commercialization of MEMS devices.

Generally, ductile materials, such as nickel, have the mechanical property of time dependence when subjected to a constant load or stress, suggesting that the strain response of the materials depends on the time-scale and the applied loading. In other words, the most important factor that dominates failure mechanisms is the time-stress or/and time-temperature dependent nature of the constitutive materials of the device structure. Thus, ignoring the creep mechanism in the design of microdevices will lead to the overestimation of stress and the underestimation of the strain of structure components.[16,17] However, improvement in the analysis accuracy of the time-dependent reliability of microdevices depends highly on the complete understanding of possible failure mechanisms and factors influencing their lifetime. Essential to the development of realistic stress and failure analysis, simulation models are the constitutive relations for various thin-film materials used in MEMS devices.[18–20]

The current understanding of material creep is based on bulk metals. Constant axial load has been employed as the conventional creep test for bulk materials with dimensions above the millimeter scale.[21,22] However, it is difficult to prepare a test sample and to apply load to conduct the conventional (constant axial load) creep test for thin-film materials. Hence, the creep effect of a micromachined structure has rarely been reported. Various techniques for the determination of thin film mechanical properties such as elastic modulus, hardness, yielding strength, and fracture toughness have been reported[23–27] and much of the earlier studies[28,29] have been carried out to evaluate the time-dependent properties of thin films by the on-chip self-testing method. However, these research studies have some problems such as the limitation of fabricated process and the effect of residual stresses, and seldom focus on the effect of stress level on the bending creep behaviors of thin films.

Presently, the nanoindentation system has been extensively used for measuring the mechanical properties of thin film such as elastic modulus and hardness.[30] The nanoindentation technique has several advantages over other methods. For instance, it is convenient to prepare the sample for testing. The wafer-level test is available using the nanoindentation system. In addition, the distribution of the thin film mechanical properties on the wafer surface can also be characterized. Furthermore, the load-deflection test using different apparatuses is available for free-standing micromachined beams and membranes. It is possible to characterize the mechanical properties of micromachined structures such as the stiffness, fracture toughness and residual stress.[31–34] Although there are many publications on nanoindention application, only a few reports

show the measurement of the time-dependent properties of thin films.[35,36] Thus, to establish the design criteria and life assessment methods for nickel microbeams, in this study, we aim to investigate the mechanical behavior of electroplated nickel film using the bending micromachined cantilever approach. The mechanical properties and bending creep measurements were determined using a nanoindentation loading system.

2. Analysis

In this study, a commercial nanoindention system, as shown in Fig. 1, was exploited to perform the load-deflection bending test on micromachined beams.[33,37] To determine the Young's modulus E and the yielding strength σ_y of a thin film using the bending test in Fig. 1, the probe is placed at the free end of the cantilever. After measuring the load P and the displacement δ of the probe at this particular point, the Young's modulus E of the thin film can be extracted from

$$E = 4L_e^3 / wt^3 (P / \delta), \tag{1}$$

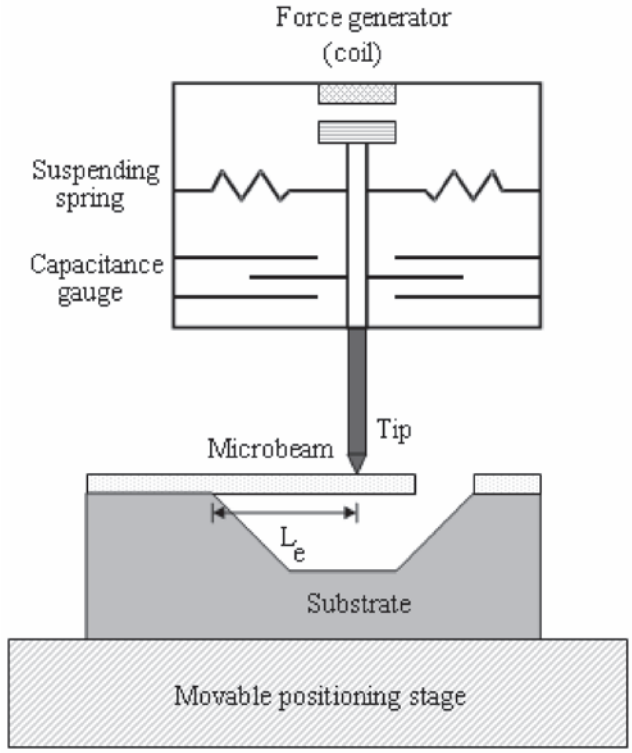

Fig. 1. Schematic for bending testing of microcantilever beam by nanoindentation system.

where w and t are the width and thickness of the cantilever beam, respectively. In addition, L_e is the length between the loading position and the fixed end of the cantilever. In eq. (1), the parameter P/δ is defined as the contact stiffness (or bending stiffness). According to the transverse load P, the distribution of normal stress σ_x at the fixed end of the cantilever is expressed as

$$\sigma_x = 12PL_e / wt^3 y, \tag{2}$$

where y is the distance from the neutral axis. Thus, the maximum normal stress σ_m resulting from the transverse load P is given as

$$\sigma_m = 12PL_e / wt^2, \tag{3}$$

The yielding load P_y can be determined from the tested cantilever beam been occurring the plastic deformation. Consequently, the yielding strength σ_y is determined after substituting P_y into eq. (3).

On the other hand, Fig. 2 shows the typical creep response of a material subjected to a constant stress. Deformation at high loading can be divided into three regimes: instantaneous (elastic) strain, secondary (steady-state) creep, and tertiary creep. In the secondary creep stage, the deformation reaches a steady state, where the strain rate ($d\varepsilon/dt$) is a constant. As shown in Fig. 2, the steady-state creep test data as a function of stress and temperature in both constant load and constant stress tests, is normally represented by a power function of stress, and temperature by an Arrhenius expression including an activation energy term (Q) derived from the chemical reaction rate theory[38]

$$d\varepsilon / dt = A\sigma^n \exp(-Q / RT), \tag{4}$$

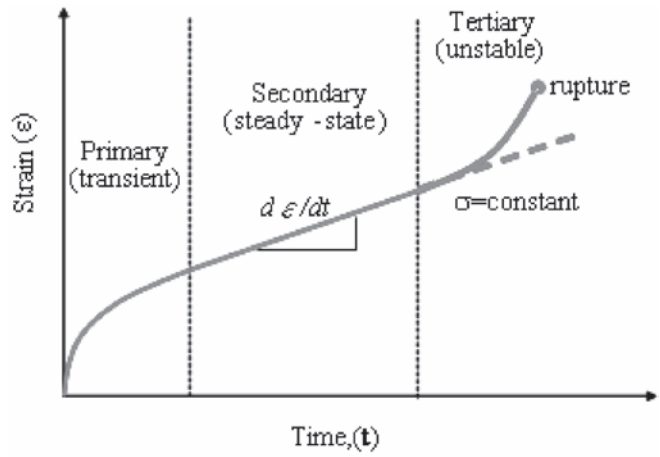

Fig. 2. General schematic of creep behavior.

where A, which is a constant, depends on the structure; n is the stress exponent; and R is the Boltzmann's constant. This equation can be used to describe the linear relationship (n=1) between the creep strain rate and the applied stress (or normalized stress σ/E) at any given temperature. Although an exponential or hyperbolic sine stress function may provide a better fit in some cases, the power function of stress has generally prevailed and become strongly linked with mechanistic treatments.

3. Experimental Procedure

3.1 *Sample fabrication*

Nickel microcantilever beam specimens were prepared by microlithography and electroplating techniques. The fabrication process is shown in Fig 3. First, an insulation SiO_2 layer was thermally grown on a (100) Si wafer, as shown in Fig. 3(a). Then, Ti/Ni films with a 100/200 nm thickness were deposited by evaporation as an adhesive layer and a seed layer, respectively, as shown in Fig. 3(b). After that, the thick photoresist AZ 4620 was spinned on a silicon substrate and patterned, as shown in Fig. 3(c). Then,

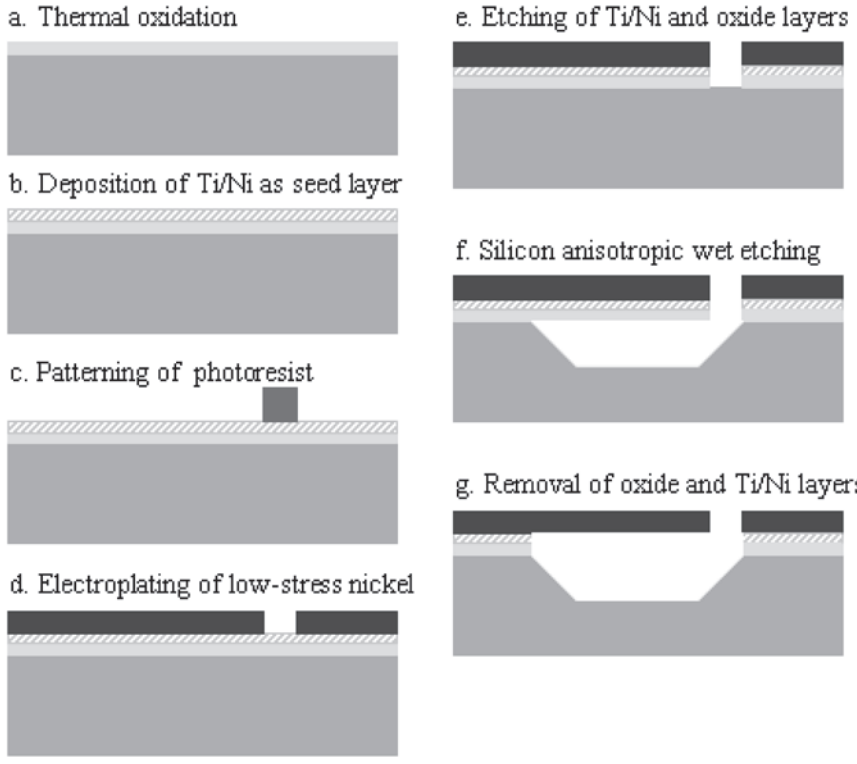

Fig. 3. Fabrication process of test nickel cantilever beam.

the nickel film was electroplated and the photoresist was removed by acetone, as show in Fig. 3(d). The detailed properties of the nickel electroplating bath are listed in Table 1. For the next step, the etching windows of the silicon surface were opened by etching the adhesive and seed layers, as shown in Fig. 3(e). Finally, the nickel cantilevers were freely suspended on the substrate after bulk silicon etching by N_2H_4, and both the adhesive and seed layers were removed by wet etching, as shown in Figs. 3(f) and 3(g), respectively. In this experiment, the designed micromachined cantilevers were 10 μm wide and 2 to10 μm thick, and their lengths ranged from 20 to 150 μm.

According to the electroplating properties listed in Table 1, the electroplating of nickel films was carried out in a nickel sulfa mate bath. Figure 4 shows the experimental result of film thickness as a function of the electroplating time. It is shown that film thickness increases approximately linearly with the electroplating time. Moreover, the grain size of the specimen was approximately 200 to 300 nm as observed from the FEM micrograph shown in Fig. 5. Figure 6 shows the SEM image of the typical fabricated micromachined nickel cantilever beams. Before testing, an optical interferometer has been used to measure the surface profile of the fabricated micromachined cantilever. However, even a beam with thickness of 2 μm and length of 150 μm, the measured out-of-plane deformation along the beam length is uniform so that the residual stress effect can be neglected. On the other hand, the etching selectivity of Ni to Si is extremely large in N2H4, the measured thickness variation of the Ni film was much less than 0.1 μm after bulk silicon etching.

3.2 *Experimental setup*

The experiment setup containing the commercial nanoindentation system is shown in Fig. 1. The commercial nanoindentation system is mainly composed of a magnetic loading actuator, a capacitive displacement sensor, a probe, and supporting springs. The force resolution of the loading actuator is approximately at sub-μN load scale, and the displacement sensing resolution of the capacitive sensor is within the nanometer length-

Table 1
Properties of nickel electroplating bath for sample fabrication.

Ni $(NH_2SO_3)+4H_2O$	182 g/l
Ni (as metal)	10 kg
Boric acid	40 g/l
Aerosol	1 g/l
Saccharin	8.3 g/l
Wetting agent	0.3 %/vol
Temperature	50°C
pH	3.9–4.0
Anode	Sulfur-depolarized nichel in Ti basket with PTFE bag
Current density	5 mA/cm^2
Voltage	5 V

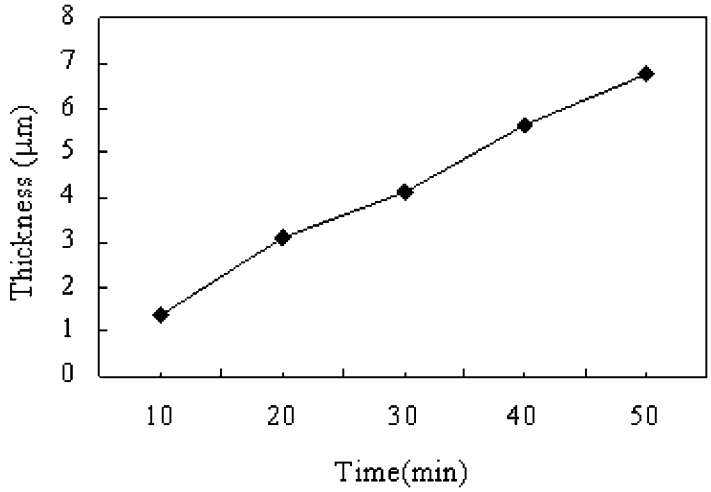

Fig. 4. Electroplated thickness of the nickel films for different fabrication times.

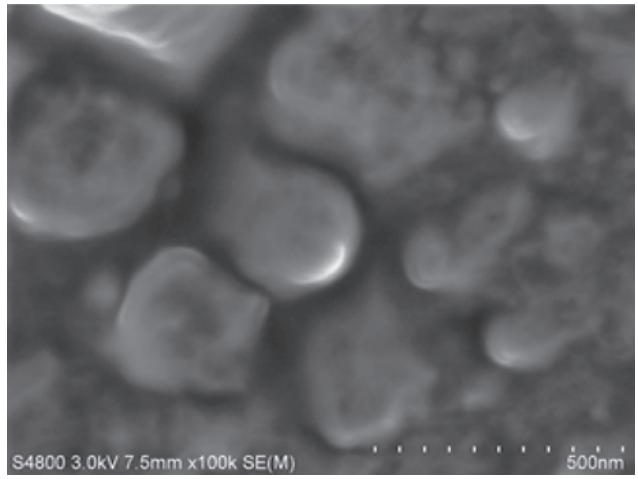

Fig. 5. FEM micrograph of grain size of electroplated nickel film..

scale. In addition, the displacement resolution of the moving stage is approximately ±1.5 μm. The needle with the Berkovich triangular pyramidal tip that made from diamond is used as the probe for the indenter. Thus, the deformation can be neglected during testing. The system employs an XY stage to position the sample directly underneath the tip of the probe. After been driven downward by the loading actuator, the probe will apply a load on the film surface. This instrument monitors and records the dynamic load and displacement of the probe during measurement. The materials are characterized by continuously recording the measured data.

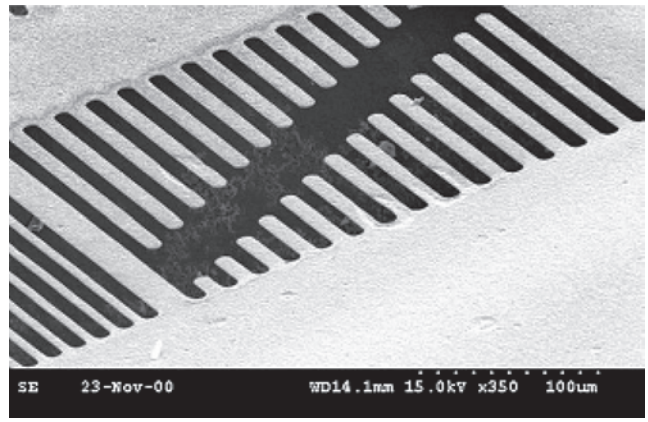

Fig. 6. The SEM image of electroplated nickel microbeams with different equivalent length.

4. Experimental Results and Discussion

In this study, both bulk micromachining and electroplating techniques were employed to fabricate test nickel cantilevers for measuring mechanical properties and creep behavior. A commercial nanoindentation system was used to perform the load-deflection test for micromachined cantilevers. It is noted that in this study have considered and eliminated the effect of the indentation depth of probe tip into thin film during the bending test of the microcantilever by referring to the databases of the indentation test.[39]

4.1 *Mechanical properties*

4.1.1 *Bending test*

As shown in the measurement setup in Fig. 1, the moving rate of the tip downward is set to be 30 nm/s during the experiment so as to meet the quasi-static testing. A typical measurement result of the variation of displacement with the applied loading-unloading is shown in Fig. 7(a). In this case, the measured specimen dimensions using the 3-D optical interferometer were 10.1 μm thick and 11.5 μm wide, and the equivalent length of the set up is 100 μm, oriented from the fixed end of the microbeam. Figure 7(a) can be reorganized to the variation in beam stiffness with the displacement, as shown in Fig. 7(b). Figure 7(b) indicates that beam stiffness approaches a constant untill the yield point occurs, and then getting worse after plastic deformation developed. Thus, substituting the measured cantilever stiffness P/δ in elastic deformation and its geometry parameters into eqs. (1) and (3), the Young's modulus and the yielding strength can be determined. The calculated value for the Young's modulus E and the yielding strength σ_y of the electroplated nickel film for the number of ten indent-points are in the ranges of 179 to 199 GPa (average 191 GPa) and 0.66 to 1.12 GPa (average 0.79 GPa), respectively.

Previously researches for the mechanical properties of an electroplated nickel film are listed in Table 2.[4,6,9,40,41] It is observed that the Young's modulus and yielding strength

(a)

(b)

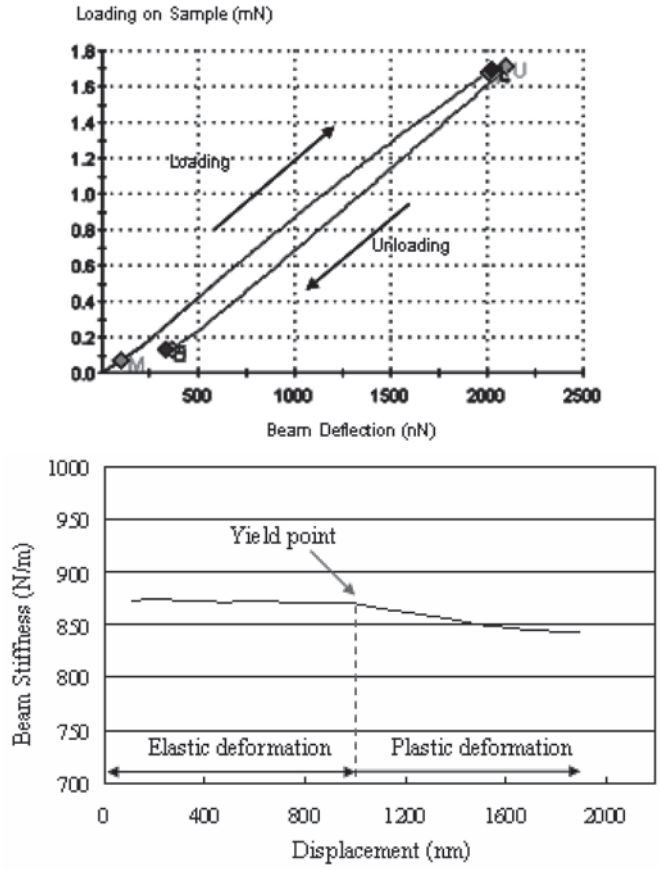

Fig. 7. Typical measured results of microcantilever bending test: (a) load vs deformation, and (b) contact stiffness vs deformation.

vary significantly as a result of differences in specimen configuration and size. The specimens with smaller dimensions have superior mechanical properties. This means that the mechanical properties of thin film materials are usually not the same as those of bulk materials. In other words, electroplated nickel films have different mechanical behaviors from their bulk counterparts because of the differences in materials properties. Thus, bulk properties can not be suitably adopted for predicting and characterizing the reliability of microstructures made from thin film materials.

4.1.2 *Indentation test*

To verify and compare the measured results of the bending test, we also used the nanoindenation system to measure the elastic modulus and hardness of the electroplated nickel film for different thicknesses by indentation testing. The measurement mechanism is shown in Fig. 8(a). As the indenter is driven into the material, both elastic (h_c) and

Table 2
Electroplated Nickel Young's modulus and yielding strength reported from previously technique articles and this research.

Reference	Test method	Specimen cross section (width × thickness)	E(GPa)	σ_y (MPa)
40	Tensile	Diameter = 1.6 mm	160	277
6	Tensile	200 × 200 μm^2	176	323
9	Tensile	200 × 20 μm^2	202	405
41	Tensile	14 × 6 μm^2	231	1550
4	Bending	160 × 160 μm^2	125	NA
Present study	Bending	10 × 10 μm^2	205	660–1120

plastic (h_s) deformations cause the formation of hardness impression conforming to the shape of the indenter to some contact depth. As the indenter is withdrawn, only the elastic portion of the displacement is recovered. From the recovered material, elastic modulus is determined. A typical load-displacement curve is demonstrated in Fig. 8(b). As shown in the figure, the indenter load is increased from zero (S) to a certain maximum value P_{max}, and then gradually decreases to zero.

According to the experimental results in Fig. 8 and the indentation theorem,[42,43] the variations in the Young's modulus and hardness with indentation depth are shown in Figs. 9(a) and 9(b), respectively. It is shown that the Young's modulus and hardness change drastically in the beginning due to the surface profile of the indentation point. According to the substrate effect, elastic modulus varies with indentation depth. A conservative rule of thumb is that the depth of the contact should be less than 10% of the thin-film thickness, although some materials have been claimed for depths of up to 25%.[16] Thus, in fair agreement with the results mentioned previously, the Young's modulus and hardness of the electroplated nickel film considered at the ranges of 5% and 10% of thickness are 205±13 GPa and 1.52±0.065 GPa, respectively. In addition, the measured Young's modulus for the electroplated nickel micromachined beams with different thicknesses is shown in Fig. 10.

By comparing the measured Young's modulus of bending and indentation tests, their difference is only approximately 5%. It is evident that the bending test results in this experiment are reliable. In addition, the measured results shown in Fig. 10 reveal that the variations in Young's modulus are not significant with film thickness. This means that the mechanical properties of electroplated nickel films within a range of 2 to 10 μm are uniformity.

4.2 *Creep test*

According to the measured yielding strength σ_y of 0.79 GPa, various stress levels from 43%σ_y (0.34 GPa) to 87%σ_y (0.69 GPa) were applied to the cantilever for the bending creep test. Presently, the testing duration is set to be 360 min under constant temperature. During the tests, the temperature is kept at 24°C and the relative humidity

(a)

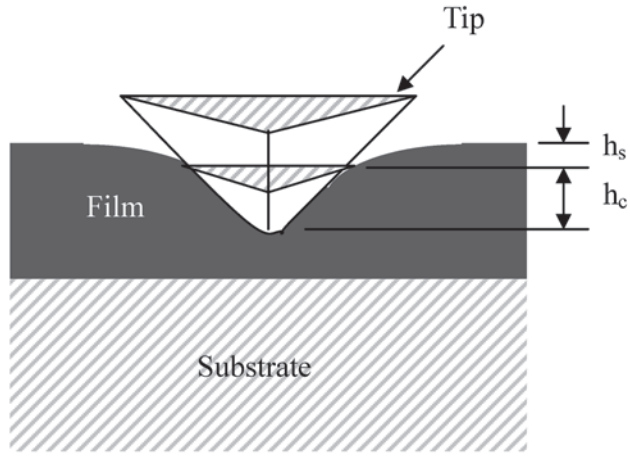

(b)

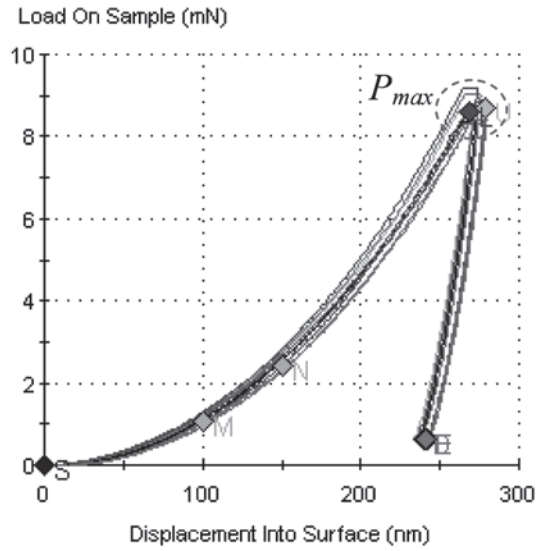

Fig. 8. (a) Schematic diagram of indentation test. (b) Measured load-displacement curves of electroplated nickel film.

is set at 50% to ensure a thermal drift rate under 0.02 nm/s. The typical measurement results regarding the variations in load, deflection, and time are shown in Fig. 11. If creep behavior occurs, the deflection and strain of the cantilever will vary with loading time, even though the applied load is a constant. Hence, the creep of thin films can be characterized by the strain-time data of microcantilevers, as shown in Fig. 12. It is shown that most of the strain-time curves in Fig. 12 have only two different stages, namely primary (transient) and secondary (steady-state) stage. The tertiary stage did not occur in the strain-time data until the applied load exceeded 87%σ_y (in the case of 0.69 GPa). In these cases, the behavior of the material itself is not changed. However, the

(a)

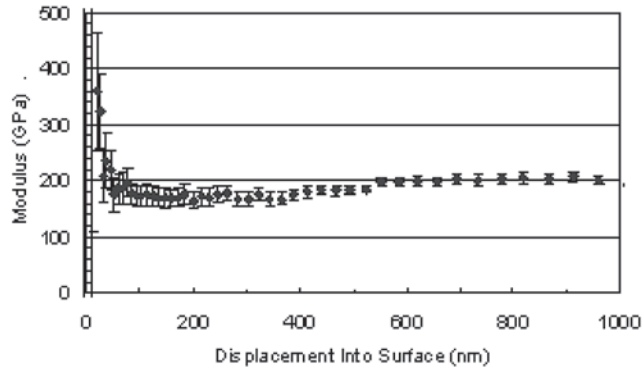

(b)

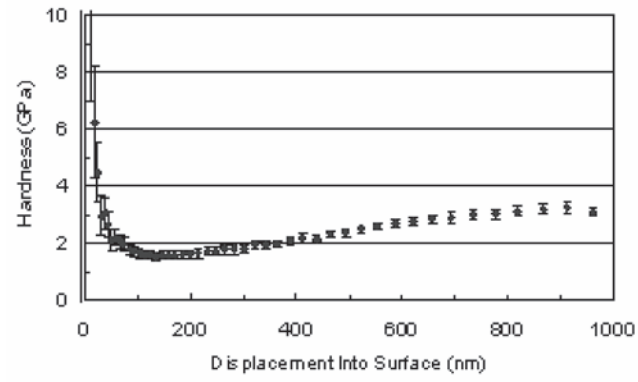

Fig. 9. Measurement results of electroplated nickel film using indentation method: (a) modulus vs displacement into surface, and (b) hardness vs displacement into surface.

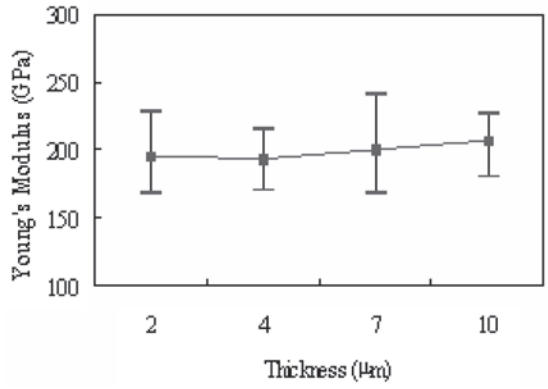

Fig. 10. Elastic modulus of the electroplated nickel films for different thicknesses.

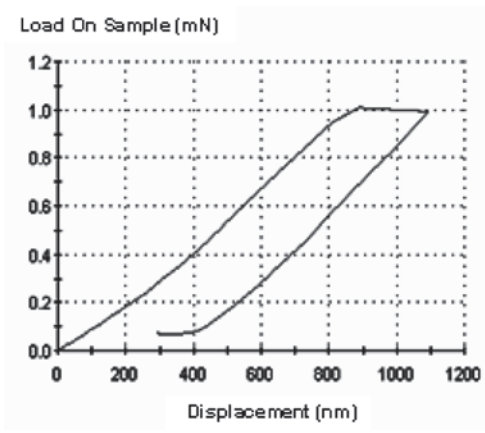

(a)

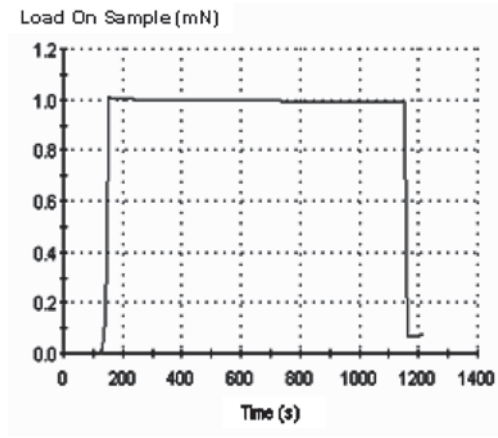

(b)

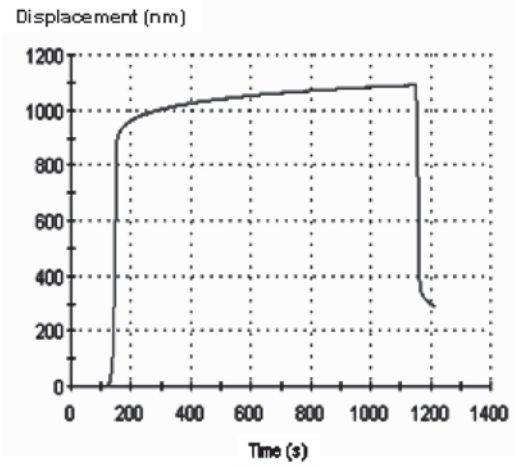

(c)

Fig. 11. Typical measurement results of time-dependent bending test: (a) load vs displacement curve, (b) load vs time curve (c) displacement vs time curve.

cross-sectional area of the cantilever is decreased.

The steady-state strain rate of the electroplated nickel film associated with a particular stress can be obtained from Fig. 12. From these curves, creep strain rate can be determined at any given time by taking the derivative of the creep curve. The minimum rate was taken as the creep rate of the steady-state stage. Note that in the early decelerating transient creep stage, creep strain rate starts from a high value and decreases to the steady-state value $d\varepsilon/dt$ as the material work hardens.

According to the theory of the bending of beams, the strain ε can be express as a function of the beam geometries (equivalent length L_e and thickness t) as well as the

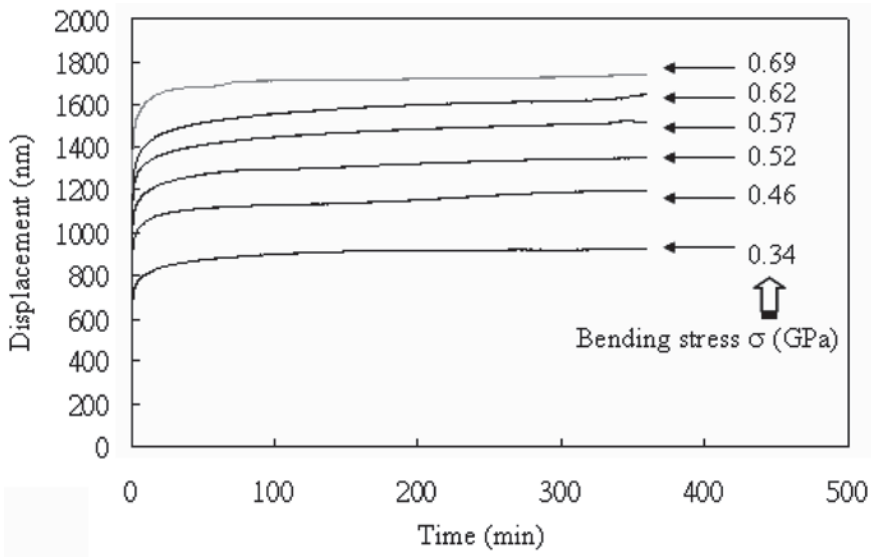

Fig. 12. Strain vs time (duration is 6 h) of bending creep testing at various stress levels.

displacement δ. Hence, according to the parameters of the tested microbeams and the measured displacement variation in Fig. 12 as well as the linear curve fitting of the steady-state stage, the variation in steady-state strain rate with stress is summarized in Fig. 13. As the bending stress is smaller than yielding strength σ_y (<0.79 GPa), the relation between stress and strain rate can be expressed as: $(d\varepsilon/dt) = 0.0016e^{2.5(\sigma)}$. This function from the curve fitting with the R^2 equal to 0.98 provided a better fit although other functions such as linear function may provide different fitting results. The slope of the curve varies with the stress levels nonlinearly, and there exist a slight variation between different stress levels. In relation to eq. (4), it is clear that the Norton's power law creep equation was unsuitable to describe the creep behavior in this case. However, according to the relations between stress and strain rate, the bending creep behavior of a 10 μm thick electroplated nickel microbeam under a constant temperature was characterized.

5. Conclusion

In this study, we have successfully investigated a bending test for electroplated nickel films using the micromachined bending cantilever approach. The bending creep test of a 10 μm thick electroplated nickel film was performed and characterized using a nanoindentation loading system. Based on both bending and indentation tests, the measured Young's modulus and yield strength of the electroplated nickel films with thicknesses from 2 to10 μm are approximately 200 GPa and 0.8 GPa, respectively. When the induced bending stress is more than the yielding strength, beam stiffness

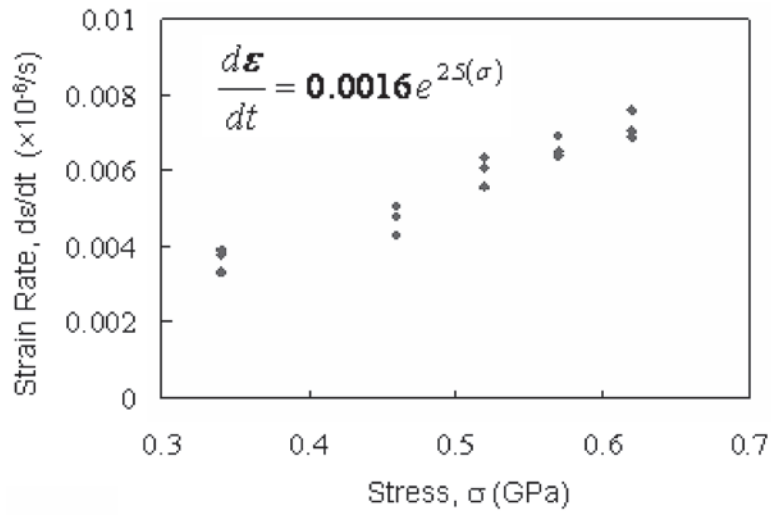

Fig. 13. Variation in steady-state strain rate with stress.

would be worse. Based on the results of bending creep behavior, as the bending stress σ is smaller than σ_y, the relation between stress and strain rate is suitable expressed as: $(d\varepsilon/dt) = 0.0016e^{2.5(\sigma)}$. The test results reported herein have important implications for the development of reliable MEMS/IC devices.

Acknowledgements

This project was (partially) supported by the National Science Council of Taiwan under grant of NSC-95-2221-E-035-016. The authors appreciate the NSC Central Regional MEMS Center (Taiwan), the Nano Facility Center of National Tsing Hua University, the Precision Instrument Support Center of Feng Chia University, and the NSC National Nano Device Laboratory (NDL) for providing the fabrication facilities.

References

1 J. D. Williams and W. Wang: Microsystem Technologies **10** (2004) 699.
2 J. Wu and G. H. Bernstein: Journal of Vac. Sci. Technol. B **22** (2004) 611.
3 J. A. van Kan, I. Rajta, K. Ansari, A. A. Bettiol and F. Watt: Microsystem Technologies **8** (2002) 383.
4 L. S. Stephens, K. W. Kelly, S. Simhadri, A. B. McCandless, and E. I. Meletis: Journal of MEMS **10** (2001) 347.
5 K. P. Larsen and J. T. Ravnkilde: IEEE MEMS'2002 Conference (2002) p. 443.
6 W. N. Sharpe, D. A. La Van and R. L. Edwards: Proc. Int. Conf. Solid-State Sensors and Actuators (Chicago, 1997) p. 607.
7 H. S. Cho and K. J. Hemker: EEE MEMS'2002 Conference (2002) p. 439.

8 S. H. Yi, F. J. von Preissig and E. S. Kim: Journal of MEMS **11 (**2002) 293.
9 E. Mazza, S. Abel and J. Dual: Microsystem Technologies **2** (1996) **197**.
10 R. Ballarini: Mat. Res. Soc. Symp. Proc. **546** (Boston, 1998) p. 3.
11 T. Namazu, Y, Isono and T. Tanaka: Journal of MEMS **9** (2000) 450.
12 T. Tsuchiya, O. Tabata, J. Sakata and Y. Taga: Journal of MEMS **7** (1998) p. 106.
13 T. Yi, L. Li and C. J. Kim: Sensors and Actuators **83** (2000) 172.
14 W. N. Sharpe, K.M. Jackson, K. J. Hemker and Z. Xie: Journal of MEMS **10** (2001) 317.
15 X. Li, T. Ono, Y. Wand and M. Esashi: IEEE MEMS'2002 Conference (2002) p. 427.
16 B. D. Jensen, K. Saitou, J. L. Volakis and K. Kurabayashi: IEEE Microwave and Wireless Components **13** (2003) p. 364.
17 O. Kraft, R. Schwaiger and P. Wellner: Materials Science and Engineering A **319–321** (2001) 919.
18 W. M. van Spengen, R. Puers, R. Mertens and I. D. Wolf: J. Micromech. Microeng. **14** (2004) 514.
19 J. Cotton, J. W. Grant, M. K. Jensen and B. J. Love: Journal of Adhesion & Adhesives **21** (2001) 65.
20 K. S. The and L. Lin: Journal of Microelectronics **30** (1999) 1169.
21 J. Li, and A. Dasgupta: IEEE Transactions on Reliability **42** (1993) p. 339.
22 H. S. Cho, K. J. Hemker, K. Lian, J. Goettert and G. Dirras: Sensors and Actuators A **103** (2003) 59.
23 A. Llzhofer, H. Schneider and C. Tsakmakis: Microsystem Technologies 4 (1997) p. 46.
24 W. C. Oliver and G. M. Pharr: J. Mater. Res. **7** (1992) 1564.
25 S. B. Brown, G. Povirk and J. Connally: IEEE MEMS'93 Conference (1993) p. 99.
26 J. H. Zhao, T. Ryan and P. S. Ho: Journal of Applied Physics **88** (2000) 3029.
27 W. N. Sharpe, B. Yuan and R. L. Edwards: Journal of MEMS **6**, (1997) p. 193.
28 K. P. Larsen, A. A. Rasmussen and J. T. Ravnkilde: Sensors and Actuators A **103** (2003) 156.
29 D. R. Sparks, M. I. Chia and G. Q. Jiang: Sensors and Actuators A **95** (2001) 61.
30 G. M. Pharr and W. C. Oliver: MRS Bulltin **7** (1992) p. 28.
31 K. P. Larsen and J. T. Ravnkilde: IEEE MEMS'2002 Conference (2002) p. 443.
32 S. Johansson and J. A. Schweitz: J. Appl. Phys. **63** (1988) 4799.
33 T. P. Weihs, S. Hong, J. C. Bravman and W. D. Nix: Mat. Res. Soc. Proc. **130** (1989) 87.
34 J. Qian, T. X. Yu and Y. P. Zhao: Microsystem Technologies **11** (2005) 97.
35 K. B. Yoder, D. S. Stone, J. C. Lin and R. A. Hoffman: Materials Research Society Symposium Proceedings **356** (1995) 651.
36 V. Raman and R. Berriche: Journal of Materials Research **3** (1992) 627.
37 S. Asyf, K. J. Wahl, and R. J. Colton: Rev. Sci. Inst. **70** (1999) 2408.
38 J. Li and A. Dasgupta: IEEE Transactions on Reliability **42** (1994) 339.
39 C. Hsu, C. Yu, C. Tsou and W. Fang: 2004 ASME International Mechanical Engineering Congress and Exposition (Anaheim, 2004).
40 T. Buchhit, T. Christenson, D, Schmale and D. Lavan: Proc. MRS Symposium Proceedings **546** (1998) p. 121.
41 S. Greekand and F. Ericson: Proc. MRS Symposium Proceedings **518** (1998) p. 51.
42 W. C. Oliver and G. M. Pharr: J. Mater. Res. Vol. 7 (1992) p. 1564.
43 W. C. Oliver and C. J. Mchargue: Thin Solid Film **161** (1988) 117.